Available online at www.sciencedirect.com

ScienceDirect

Procedia - Social and Behavioral Sciences 138 (2014) 521 – 530

Procedia
Social and Behavioral Sciences

The 9th International Conference on Traffic & Transportation Studies (ICTTS'2014)

A Modified Social Force Model for Pedestrian Behavior Simulation at Signalized Crosswalks

Weiliang Zeng*, Hideki Nakamura, Peng Chen

Department of Civil Engineering, Nagoya University, Furo-cho, Chikusa-ku, Nagoya 464-8603, Japan

Abstract

In this study, a microscopic simulation model is developed for pedestrian behavior analysis at signalized crosswalks. It takes into account the special characteristics of pedestrian crossing behavior, such as group evasion with surrounding pedestrians, collision avoidance with conflicting vehicles, response to signal control, and response to crosswalk boundary. The classical social force model is modified to reproduce repulsive and attractive phenomena. Furthermore, a generic calibration approach is proposed based on maximum log-likelihood estimation, which enables to identify significant parameters in a statistical way. Last, a rigorous validation is conducted to confirm the model performance in terms of collision avoidance behavior with conflicting pedestrians and vehicles.

Peer-review under responsibility of Beijing Jiaotong University(BJU), Systems Engineering Society of China (SESC).

Keywords: Pedestrian crossing behavior; Social force; Microscopic traffic simulation; Signalized crosswalk

1. Introduction

Although signalized crosswalks are operated to give pedestrians priority, more than 30% of the total traffic accident fatalities in Japan are pedestrians. Many reasons exist behind such statistics, and pedestrian risk-taking behavior is deemed as one of the critical factors. This study is part of intensive efforts to develop a microscopic simulation platform for safety assessment at signalized intersection (Dang et al., 2012). Thus, in order to develop such a simulation platform, pedestrian behavior must be reasonably reflected.

* Corresponding author. Tel.: +86-152-789-5175.
E-mail address: zeng@genv.nagoya-u.ac.jp.

Peer-review under responsibility of Beijing Jiaotong University(BJU), Systems Engineering Society of China (SESC).
doi:10.1016/j.sbspro.2014.07.233

To date, pedestrian behavior modeling has attracted considerable attention. Comparing to macroscopic models, microscopic models offer a more detailed analysis of pedestrian behavior. Generally, existing microscopic models can be classified into two categories: discrete and continuous models. The family of discrete models includes discrete choice model (Robin et al., 2009), lattice gas model (Guo and Huang, 2008) and cellular automaton model (Burstedde et al., 2001), in which space is discretized to approximate real pedestrian movement. However, pedestrians behave flexibly and the choice of next step is unrestricted dynamic, which cannot be fully taken into account by only choosing one option from a limited choice set. Continuous models use differential equations to describe the dynamic movement in space. At the early stage, a magnetic-force model was developed by borrowing a motion equation used for magnetic fields (Okazaki, 1979). Based on this concept, a more robust physical force based model, i.e., social force model, was applied to evacuation analysis (Helbing and Molnar, 1995). The physical force based model makes it possible not only to accurately describe dynamic pedestrian movement in space, but also to reproduce the self-organization phenomenon such as lane-formation (Helbing et al., 2001).

Although many studies focus on the general mechanism of pedestrian behavior, few studies shed light on the application of social force model to pedestrian behavior at signalized crosswalk. The characteristics of pedestrian behavior at signalized crosswalks, such as group evasive behavior with surrounding pedestrians, collision avoidance with turning vehicles, reaction to crosswalk boundary, and response to signal control, are important to evaluate the safety performance. However, existing models, neither fully developed nor correctly calibrated based on real trajectory data, fail to illustrate these crucial behaviors.

The main contribution of this study is the development of a microscopic model based on social force theory, which enables to consider the characteristics of pedestrian behavior at signalized crosswalks. Furthermore, an estimation approach for calibrating the social force model based on real trajectory data is proposed. Last, the validation is conducted to confirm the model performance in terms of pedestrian behavior such as collision avoidance with conflicting vehicles and surrounding pedestrians.

2. Model description

The modified social force model in this study relates five sources of social force: driving force toward destination ($\vec{F}_d$), repulsive force from surrounding pedestrians ($\vec{F}^r_{\alpha\beta}$), repulsive or attractive force from crosswalk boundary ($\vec{F}_B$), repulsive force from conflicting vehicles ($\vec{F}_v$), and attractive force from signal phase ($\vec{F}_s$). The resultant force ($\vec{F}(t_k)$) can be expressed by Eq. (1).

$$\vec{\mathbf{F}}(t_k) = \vec{\mathbf{F}}_d + \vec{\mathbf{F}}^r_{\alpha\beta} + \vec{\mathbf{F}}_B + \vec{\mathbf{F}}_v + \vec{\mathbf{F}}_s \tag{1}$$

2.1. Driving force

As shown in Fig. 1(a), the first term of Eq. (1) represents the motivation to move forward. The desired direction ($\vec{e}_\alpha$) is defined by the current position and the exit position at crosswalk, toward which pedestrians desire to move. However, pedestrians change their speed vectors dynamically due to the stimulus of surrounding environment. A deviation of the current speed vector ($\vec{v}_\alpha$) from the desired speed vector ($v^d_\alpha \vec{e}_\alpha$) leads to a force to recover to the desired speed vector within a certain relaxation time (τ_α). Therefore, the driving force can be presented by Eq. (2).

$$\vec{\mathbf{F}}_d = \frac{1}{\tau_\alpha}\left(v^d_\alpha \vec{\mathbf{e}}_\alpha - \vec{\mathbf{v}}_\alpha\right) \tag{2}$$

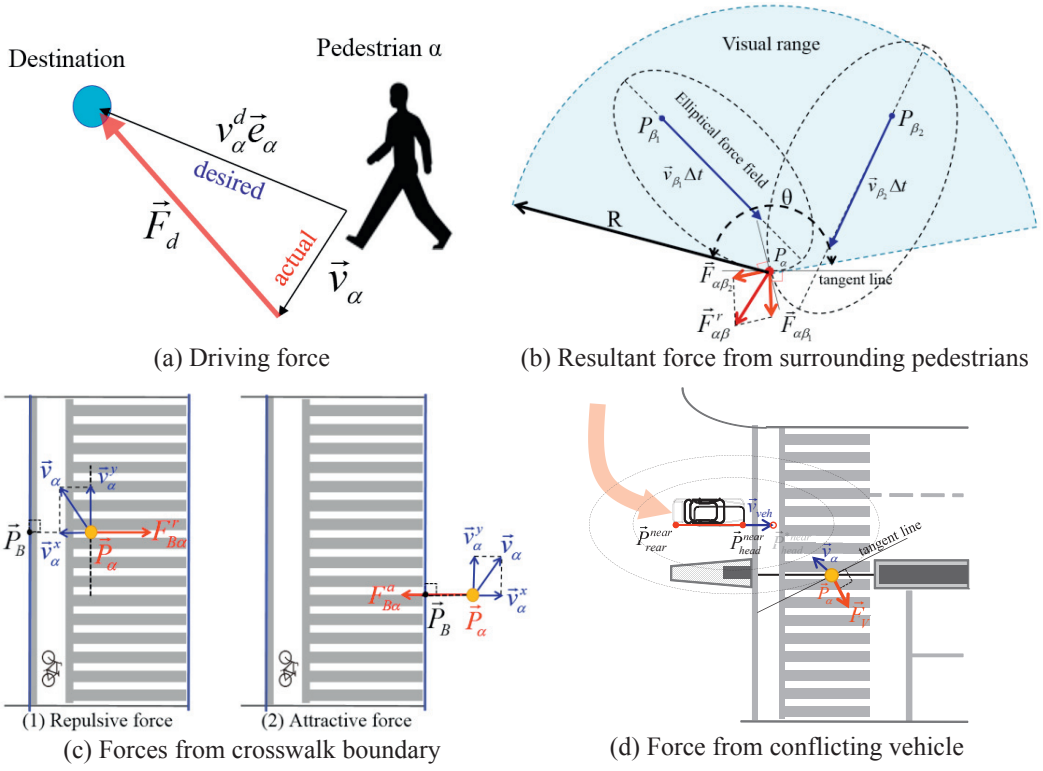

(a) Driving force

(b) Resultant force from surrounding pedestrians

(c) Forces from crosswalk boundary

(d) Force from conflicting vehicle

Fig. 1. Sources of social force at crosswalk

2.2. Repulsive force from surrounding pedestrians

The second term of Eq. (1) represents the interactions to surrounding pedestrians. It is assumed that each conflicting pedestrian within the subject pedestrian's visual range will generate an elliptical force field that results in repulsive effect to the subject pedestrian. Different from the classical social model, in this study not only the relative distance but the relative time ($T_{\alpha\beta}$) to the conflict point are considered as the influential factors to the repulsive force. As shown in Fig. 1(b), the resultant force ($\vec{F}^{r}_{\alpha\beta}$) of conflicting pedestrians can be presented by Eq. (3).

$$\vec{\mathbf{F}}^{r}_{\alpha\beta} = \sum_{i=1}^{n} A_{\beta} \exp\left[-B_{\beta} b_i - B_{\alpha\beta} T_{\alpha\beta}\right] \vec{\mathbf{n}}_{\beta_i} \tag{3}$$

where $\vec{n}_{\beta_i}$ is the normalized vector which is perpendicular to the tangent line of the elliptical force field of pedestrian β_i, A_β is the interaction strength coefficient, B_β is the interaction range coefficient for distance, $B_{\beta\alpha}$ is the interaction range coefficient for relative time, n is the number of conflicting pedestrians. And b_i is the length of semi-minor axis of the elliptical force field, which can be presented by Eq. (4).

$$b_i = \frac{1}{2}\sqrt{\left(\left\|\vec{\mathbf{P}}_{\alpha} - \vec{\mathbf{P}}_{\beta_i}\right\| + \left\|\vec{\mathbf{P}}_{\alpha} - \vec{\mathbf{P}}_{\beta_i} - \dot{\mathbf{v}}_{\beta_i}\Delta t\right\|\right)^2 - \left(\left\|\vec{\mathbf{v}}_{\beta_i}\Delta t\right\|\right)^2} \tag{4}$$

where $\vec{P}_\alpha$ is the current position of pedestrian α, $\vec{P}_{\beta i}$ is the current position of the conflicting pedestrian β_i, $\vec{v}_{\beta_i}$ is the current speed vector of pedestrian β_i, Δt is the time step in simulation.

Assume that the subject pedestrian will significantly react to the conflicting pedestrians once a potential collision is going to occur in the visual range. A potential collision can be identified by the time to conflict point (TTCP).

TTCP is defined as the expected time for two pedestrians to pass the conflict point if they keep their current speeds and directions. The TTCP for the subject pedestrian α and the conflicting pedestrian β is given by Eq. (5).

$$TTCP_\alpha = \frac{\left\|\vec{\mathbf{P}}_c - \vec{\mathbf{P}}_\alpha\right\|}{\left(\left\|\vec{\mathbf{v}}_\alpha\right\|\right)}\cos\left\langle \vec{\mathbf{v}}_\alpha, \vec{\mathbf{P}}_c - \vec{\mathbf{P}}_\alpha \right\rangle,\ TTCP_\beta = \frac{\left\|\vec{\mathbf{P}}_c - \vec{\mathbf{P}}_\beta\right\|}{\left(\left\|\vec{\mathbf{v}}_\beta\right\|\right)}\cos\left\langle \vec{\mathbf{v}}_\beta, \vec{\mathbf{P}}_c - \vec{\mathbf{P}}_\beta \right\rangle \tag{5}$$

where $\vec{P}_\beta$ is the current position of the conflicting pedestrian β, $\vec{P}_c$ is the conflicting point position.

The relative time ($T_{\alpha\beta}$) to the conflicting point in Eq. (3) can be presented by Eq. (6). Such conflict that the TTCPs of both pedestrians are positive will be deemed as valid, while negative value means that one pedestrian had passed the conflict point and no potential collision will occur.

$$T_{\alpha\beta} = \begin{cases} \left|TTCP_\alpha - TTCP_\beta\right|, \text{ if } TTCP_\alpha > 0 \text{ and } TTCP_\beta > 0 \\ +\infty, \text{ otherwise} \end{cases} \tag{6}$$

2.3. Force from boundary

Generally, pedestrians keep walking inside the boundary of crosswalk. As shown in Fig. 1(c)(1), it is assumed that when there is a velocity component toward the crosswalk boundary, a repulsive force ($\vec{F}^{r}_{B\alpha}$) will be generated. The repulsive force makes the pedestrian keep a certain distance from the boundary. However, when the pedestrian density at the crosswalk increases to some extent, some pedestrians may walk outside the crosswalk to avoid serious conflicts with others. However, most of them will move back to the crosswalk once the conflict becomes less severe. Therefore, as shown in Fig. 1(c)(2), it is assumed that an attractive force ($\vec{F}^{a}_{B\alpha}$) will attract back those pedestrians outside the crosswalk. The social force from crosswalk boundary ($\vec{F}_B$) can be presented by Eq. (7).

$$\vec{\mathbf{F}}_B = \begin{cases} \vec{\mathbf{F}}^r_{B\alpha} = A^r_B \exp\left(-B^r_B \left\|\vec{\mathbf{P}}_\alpha - \vec{\mathbf{P}}_B\right\|\right)\vec{\mathbf{n}}_{B\alpha}, \text{ if pedestrian } \alpha \text{ is inside the crosswalk} \\ \vec{\mathbf{F}}^a_{B\alpha} = A^a_B \exp\left(B^a_B \left\|\vec{\mathbf{P}}_\alpha - \vec{\mathbf{P}}_B\right\|\right)\vec{\mathbf{n}}_{\alpha B}, \text{ otherwise} \end{cases} \tag{7}$$

where $\vec{P}_B$ is the perpendicular foot point of pedestrian α on the nearest crosswalk boundary, $\vec{n}_{B\alpha}$ is the normalized vector pointing from boundary to pedestrian α, $\vec{n}_{\alpha B}$ is the normalized vector pointing from pedestrian α to crosswalk boundary. A^r_B, A^a_B, B^r_B, and B^a_B are strength coefficients to be estimated.

2.4. Force from left-turning vehicle

Because it is left-hand traffic in Japan, left-turning vehicles usually conflict with pedestrians at a permitted phase. Generally, drivers are required to yield to crossing pedestrians. However, some drivers may take risky behavior by accepting short gaps, which threaten pedestrians' safety. It is assumed that pedestrians are affected by the vehicle force field once he/she approaches it. As shown in Fig. 1(d), the pedestrian will take actions to avoid collision with the left-turning vehicle although the vehicle usually yields to the pedestrian. This situation is similar to collision avoidance with conflicting pedestrians, though the size of a left-turning vehicle is much larger than that of a pedestrian. Similarly, an elliptical force field is assumed to describe the force generated by the nearest left-turning vehicle. The difference from the force field of a conflicting pedestrian is that the two focuses of the ellipse are defined by the vehicle near-side rear position ($\vec{P}^{near}_{rear}$) and the predicted vehicle near-side head position ($\vec{P}^{*near}_{head}$) in next time step. Therefore, the repulsive force from a left-turning vehicle can be presented by Eq. (8).

$$\vec{\mathbf{F}}_v = A_v \exp\left(-B_v b_v\right)\vec{\mathbf{n}}_{v\alpha} \tag{8}$$

where A_v and B_v are the strength coefficients, $\vec{n}_{v\alpha}$ is the normalized vector which is perpendicular to the tangent line of the elliptical force field of the left-turning vehicle, b_v is the length of semi-minor axis of the elliptical force field, which can be presented by Eq. (9).

$$b_v = \frac{1}{2}\sqrt{\left(\left\|\vec{\mathbf{P}}_\alpha - \vec{\mathbf{P}}_{rear}^{near}\right\| + \left\|\vec{\mathbf{P}}_\alpha - \vec{\mathbf{P}}_{head}^{*near}\right\|\right)^2 - \left(\left\|\vec{\mathbf{P}}_{rear}^{near} - \vec{\mathbf{P}}_{head}^{*near}\right\|\right)^2} \tag{9}$$

where $\vec{\mathbf{P}}_{head}^{*near}$ can be presented by Eq. (10).

$$\vec{\mathbf{P}}_{head}^{*near} = \vec{\mathbf{P}}_{head}^{near} + \vec{\mathbf{v}}_{veh}\Delta t \tag{10}$$

where $\vec{v}_{veh}$ is the current speed vector of the conflicting vehicle.

2.5. Force from signal

Pedestrian behavior also gets influenced by the attractive force from signal control. Empirical analyses (Zhang et al., 2013) indicate that pedestrian speeds are significantly higher at pedestrian flashing green (PFG) phase than that at pedestrian green phase (PG). The possible reason is that pedestrians need to finish crossing before the onset of the red signal as soon as possible. Here, it is assumed that if the pedestrian is still on the crosswalk when the signal has changed to PFG or Red, he/she will accelerate and cross as fast as possible. The attractive force ($\vec{\mathbf{F}}_s$) from the signal can be presented by Eq. (11).

$$\vec{\mathbf{F}}_s = \begin{cases} \left(-A_s\left\|\vec{\mathbf{P}}_\alpha - \vec{\mathbf{P}}_{dest}\right\| + B_s\right)\vec{\mathbf{e}}_\alpha, & \text{if the signal phase is PFG or Red} \\ 0, & \text{otherwise} \end{cases} \tag{11}$$

where A_s and B_s are the strength coefficients, $\vec{\mathbf{P}}_{dest}$ is the destination position of the subject pedestrian α.

3. Calibration methodology

At the early stage, model parameters are usually calibrated by comparing aggregate outcomes such as speed-density relationship (Seyfried et al., 2006), or emerging pedestrian movement patterns such as lane formation (Helbing et al., 2000). However, it is still unclear if a microscopic model is able to describe individual walking behavior accurately with a macroscopic calibration method, because the aggregate outcomes only provide a reasonable average prediction (Hoogendoorn and Daamen, 2006). Recently, as the calibration of microscopic pedestrian models has been considered as important pursuit, some researchers, such as (Daamen and Hoogendoorn, 2012) and (Ko et al., 2013), have calibrated social force models by the maximum log-likelihood estimation method which is able to describe the parameters in a statistical way. The calibration methodology adopted in this study is similar to that used by (Hoogendoorn and Daamen, 2006). The only difference is that this study separates the parameters into two groups, i.e., measurable parameters and non-measurable parameters, and estimates them by maximum likelihood estimation (MLE) based on observed dataset.

3.1. Data acquisition

The north crosswalk at Kanayama intersection in Nagoya City, Japan is chosen as study site. The positions of pedestrians and left-turning vehicles were manually extracted from the video every 0.5s by using an image processing software (Suzuki and Nakamura, 2006). The dataset consists of the trajectories of 1,352 pedestrians and 124 left-turning vehicles. In total, 97,200 position samples are available. The available observations are trajectory

profiles based on time series. From these data, all relevant quantities can be derived either directly or by applying finite differences, such as positions ($\vec{P}_\alpha(t_k)$), velocities ($\vec{v}_\alpha(t_k)$), accelerations ($\vec{a}_\alpha(t_k)$), distances between pedestrians, speed angles between pedestrians, etc.

3.2. Calibration process

The developed social force model contains various parameters. As some of them cannot be derived from the observed dataset, direct calibration is difficult for them. Here, we adopt a three-stage process to alleviate this problem. As the first step, the parameters such as visual range, which are measurable but difficult to be identified from the trajectory dataset, are estimated by referring to related studies. Secondly, the parameters such as relaxation time, which are possible to be identified from the observed dataset, are directly estimated. Finally, after fixing the above parameters, other parameters, such as the strength coefficients of each force that do not have concrete physical meanings, are derived by MLE.

3.2.1. Calibration of measurable parameters

There are four measurable parameters for calibration, i.e., angle of visual range (θ), radius of visual range (R), desired speed (v_α^d), and relaxation time (τ_α).

The visual range is defined as the radius and angle at which a given standard object can be seen with unaided eyes. Because of the limitation of data collection, it is difficult to directly estimate the visual range based on the trajectory dataset. Here, according to related studies (Guo et al., 2010; Antonini et al., 2006), the angle of visual range is set as 170° and the radius of visual range is set as 8m.

Desired speed is defined as the personal average speed if a pedestrian crosses the road without any disturbance by signal, boundary, surrounding pedestrians and vehicles. The trajectory data were collected when there were no conflicting pedestrians and left-turning vehicles at pedestrian green phases and the subject pedestrian must be inside the crosswalk, which guarantees less repulsive or attractive force influencing the subject pedestrian. The results show that the average value of desired speed is 1.6m/s and the standard deviation is 0.15 m/s.

Relaxation time is defined as the time a pedestrian recovering from current speed to the personal desired speed without any disturbance. To reduce the influence of other forces, only the dataset for desired speed estimation was used. However, the pedestrian speed still changes dynamically due to personal random decision. Here, we calculate the acceleration time period from a lower current speed to the personal desired speed as the relaxation time. If the current speed is lower than desired speed, a loop will start up to search forward and find out how many time steps passing until the speed recovers to the desired speed. According to the estimation result, the average value is 2.2s and the standard deviation is 0.5s.

3.2.2. Calibration of non-measurable parameters

After fixing the estimated measurable parameters, other parameters which are difficult to measure, i.e., A_β, B_β, $B_{\beta\alpha}$, A_B^r, A_B^a, B_B^r, B_B^a, A_v, B_v, A_s and B_s, are calibrated by MLE. The position for the next time step ($\vec{P}_\alpha(t_{k+1}|\theta_p)$) closely depends on the model parameters (θ_p) to be estimated. The estimated distance vector ($\Delta\vec{d}_\alpha^{est}(t_k|\theta_p)$) is pointing from $\vec{P}_\alpha(t_k|\theta_p)$ to $\vec{P}_\alpha(t_{k+1}|\theta_p)$. Here, it is assumed that the length of $\Delta\vec{d}_\alpha^{est}(t_k|\theta_p)$ in x direction and in y direction are normally distributed with mean (μ_x, μ_y) and standard deviation (σ_x, σ_y). (μ_x, μ_y) and (σ_x, σ_y) can be estimated from the observed distance vector ($\Delta\vec{d}_\alpha^{obs}(t_k)$). The likelihood L_k of a single prediction step, i.e., from time t_k to t_{k+1}, is related directly to the probability density function of the normal distribution as shown in Eq. (12).

$$L_k\left(\Delta d_\alpha\left(\boldsymbol{\theta}_p\right)|\mu,\sigma\right)=\frac{1}{\sigma\sqrt{2\pi}}e^{\frac{-\left(\Delta d_\alpha\left(\boldsymbol{\theta}_p\right)-\mu\right)^2}{2\sigma^2}} \tag{12}$$

Note that the distance vector ($\Delta\vec{d}_\alpha^{obs}(t_k)$) is a two-dimensional variable. To simplify the calculation, it is assumed that both vector components in x direction and in y direction are normal distributions. Therefore, $\Delta d_\alpha(\theta_p)$ is the combination of $\Delta\vec{d}_{\alpha x}^{est}(t_k|\theta_p)$ and $\Delta\vec{d}_{\alpha y}^{est}(t_k|\theta_p)$ as shown in Eq. (13). Accordingly, μ and σ in Eq. (14, 15) are

derived from (μ_x, μ_y) and (σ_x, σ_y) respectively.

$$\Delta d_\alpha\left(\boldsymbol{\theta}_p\right)=\left\|\Delta\vec{\mathbf{d}}_{\alpha x}^{est}\left(t_k\left|\boldsymbol{\theta}_p\right.\right)\right\|+\left\|\Delta\vec{\mathbf{d}}_{\alpha y}^{est}\left(t_k\left|\boldsymbol{\theta}_p\right.\right)\right\| \tag{13}$$

$$\mu=\left|\mu_x\right|+\left|\mu_y\right| \tag{14}$$

$$\sigma=\sqrt{\sigma_x^2+\sigma_y^2+2\operatorname{cov}\left(\left\|\Delta\vec{\mathbf{d}}_{\alpha x}^{est}\left(t_k\left|\boldsymbol{\theta}_p\right.\right)\right\|,\left\|\Delta\vec{\mathbf{d}}_{\alpha y}^{est}\left(t_k\left|\boldsymbol{\theta}_p\right.\right)\right\|\right)} \tag{15}$$

where $\Delta\vec{\mathbf{d}}_{\alpha x}^{est}\left(t_k\left|\boldsymbol{\theta}_p\right.\right)$ is the vector components $\Delta\vec{\mathbf{d}}_{\alpha}^{est}\left(t_k\left|\boldsymbol{\theta}_p\right.\right)$ in x direction, and $\Delta\vec{\mathbf{d}}_{\alpha y}^{est}\left(t_k\left|\boldsymbol{\theta}_p\right.\right)$ is the vector components $\Delta\vec{\mathbf{d}}_{\alpha}^{est}\left(t_k\left|\boldsymbol{\theta}_p\right.\right)$ in y direction.

Considering the entire observed samples and neglecting the correlation between subsequent samples, the likelihood of the observation given for the model parameters (θ_p) can be presented by Eq. (16).

$$L\left(\Delta d_\alpha\left(\boldsymbol{\theta}_p\right)\left|\mu,\sigma\right.\right)=\prod\frac{1}{\sigma\sqrt{2\pi}}e^{\frac{-\left(\Delta d_\alpha\left(\boldsymbol{\theta}_p\right)-\mu\right)^2}{2\sigma^2}}=\frac{\left(2\pi\right)^{-\frac{n}{2}}}{\sigma^n}\exp\left[-\frac{\sum\left(\Delta d_\alpha\left(\boldsymbol{\theta}_p\right)-\mu\right)^2}{2\sigma^2}\right] \tag{16}$$

To facilitate the computation, the logarithm is taken on both sides of Eq. (16). Therefore, the log-likelihood can be presented by Eq. (17). The maximum log-likelihood estimates of model parameters (θ_p) are obtained such that Eq. (17) is maximized.

$$\ln L=-\frac{1}{2}n\ln\left(2\pi\right)-n\ln\left(\sigma\right)-\frac{\sum\left(\Delta d_\alpha\left(\boldsymbol{\theta}_p\right)-\mu\right)^2}{2\sigma^2} \tag{17}$$

Table 1 shows the calibration result of parameter estimation. According to p values at the 95% confidence level, all the parameters in the modified social force model are significant. According to the estimation results, the coefficient for the interaction strength of vehicle repulsive force has the largest value, implying a higher sensitivity of collision avoidance with vehicles on pedestrian crossing behavior.

Table 1. Calibration results of the social force model

Parameters	Equation	Estimates	p value	Notes
A_β	(3)	0.81	0.00	Strength coefficients for repulsive force from surrounding conflicting pedestrians
B_β	(3)	0.74	0.01	
$B_{\beta\alpha}$	(3)	0.34	0.00	
A_B^r	(7)	0.23	0.00	Strength coefficients for repulsive force from crosswalk boundary
B_B^r	(7)	0.65	0.00	
A_B^a	(7)	0.51	0.00	Strength coefficients for attractive force from crosswalk boundary
B_B^a	(7)	0.93	0.00	
A_v	(8)	1.29	0.02	Strength coefficients for repulsive force from conflicting left-turning vehicle
B_v	(8)	0.96	0.00	
A_s	(11)	0.12	0.00	Strength coefficients for attractive force from PFG and Red phase signal
B_s	(11)	0.09	0.00	

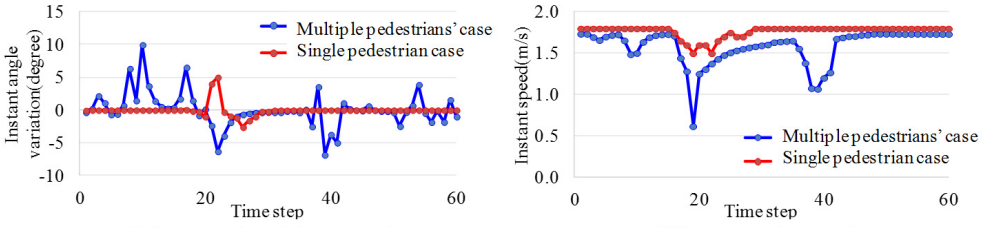

(a) Instant angle variation comparison (b) Instant speed comparison

Fig. 2. Performance of instant angle and speed in two scenarios

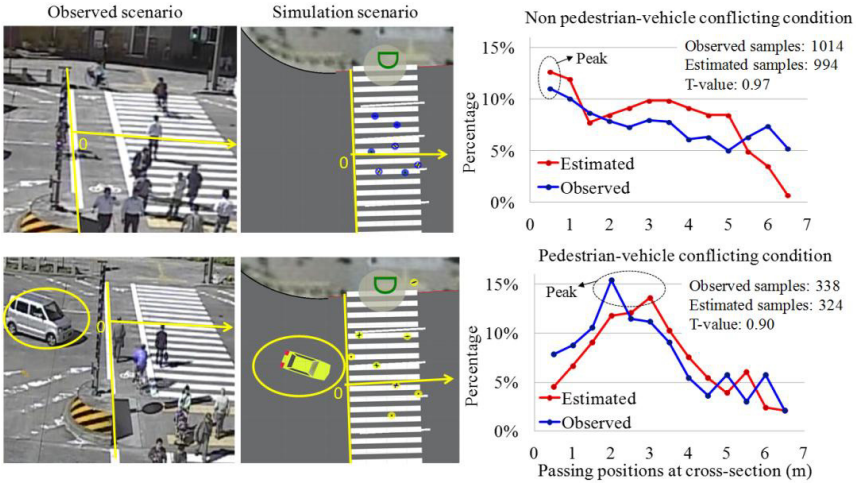

Fig. 3. Comparison of passing positions at a specified cross-section

4. Model performance

4.1. Collision avoidance with surrounding pedestrians

Two basic scenarios were set to observe the maneuver of collision avoidance with surrounding pedestrians. The subject pedestrian comes across only one conflicting pedestrian in scenario A while he/she comes across multiple pedestrians in Scenario B. Fig. 2(a) shows the comparison of instant angle variation in these two scenarios. As the red plots show, the pedestrian almost does not change the walking direction if not conflicting with others; while adjusts the instant angle to avoid collision if a potential collision is coming up. Then, the pedestrian recovers to the desired direction once the conflict disappears. The blue plots show that the subject pedestrian has to change the angle more frequently to avoid collision with multiple conflicting pedestrians. Fig. 2(b) shows the comparison of instant speeds. As the red plots show, the pedestrian keeps the desired speed if not conflicting with others. However, once someone approaches, the pedestrians will decrease the speed to avoid collision, and then recovers to the desired speed once passing the conflicting point. The blue plots show that the subject pedestrian has to decelerate and accelerate more frequently when conflicting with multiple pedestrians.

4.2. Collision avoidance with conflicting vehicle

To analyze the interaction with left-turning vehicles, two conditions are set. One is pedestrian-vehicle conflicting condition, which means that turning vehicles exists at or are approaching the crosswalk when pedestrians are crossing, while the other is no pedestrian-vehicle conflicting condition, which means that no conflicting vehicles

exist when pedestrians crossing. As shown in Fig. 3, a specified cross-section, the central line of the third vehicle lane (from the curb of the exit approach), is chosen for analysis because the pedestrian vs. vehicle conflict occurs most frequently along this exit lane according to the observed dataset. It is shown that the peak of the histogram in observed dataset shifts from 0 to 2m if the pedestrian comes across left-turning vehicles. This phenomenon indicates that pedestrians are likely to detour to avoid collision with vehicles. According to t-test at the 95% confidence interval, no significant difference was found between observed and estimated passing positions. It demonstrates that the developed model can well present the behavior of collision avoidance with vehicles. Note that the peak of the histogram in estimated dataset shifts from 0 to 3m, which indicates that the reaction of pedestrian in simulation is a little more sensitive than that in real situation. Therefore, the repulsive force from turning vehicle still needs to be improved in the future.

5. Conclusions and future work

Based on social force theory, a modified social force model considering the typical pedestrian behaviour at signalized intersection, e.g., group evasive maneuver, collision avoidance with turning vehicles, reaction to crosswalk boundary, and response to signal, was developed. It not only possesses the advantage of the classical social force model, but also enables to reflect the characteristics of pedestrian behaviour at signalized crosswalk.

Then, the developed model was incorporated into simulation. The maximum log-likelihood estimation was applied to the parameter calibration. The validation indicated that this model can well reproduce the collision avoidance with vehicles and surrounding pedestrians as in the real world. Therefore, the proposed model offers a good basis for intersection safety assessment by simulation.

Still, there are several problems needing further attention in future work. For example, the reaction to vehicle is a little more sensitive than that in real world. In addition, the pedestrian characteristics such as age, gender, and partner relationship should also be considered as the influencing factors of crossing behavior. These limitations will be improved by a more elaborate modeling approach and a more strict calibration procedure in our future work.

Acknowledgements

The authors are very grateful to Committee on Advanced Road Technology (CART) of Road Bureau, Ministry of Land, Infrastructure, Transport and Tourism (MLIT) for great support to this research.

References

Antonini, G., Bierlaire, M., & Weber, M. (2006). Discrete choice models of pedestrian walking behavior. *Transportation Research Part B*, 40, 667 - 687.

Burstedde, C., Klauck, K., Schadschneider, A., & Zittartz, J. (2001). Simulation of pedestrian dynamics using a two-dimensional cellular automaton. *Physica A*, 295, 507 - 525.

Dang, M.T., Alhajyaseen, W.K.M., Asano, M., & Nakamura, H. (2012). Development of microscopic traffic simulation model for safety assessment at signalized intersections. *Transportation Research Record* 2316, 122 - 131.

Daamen, W., & Hoogendoorn, S. P. (2012). Calibration of pedestrian simulation model for emergency doors for different pedestrian types. *Transportation Research Record*, 2316, 69 - 75.

Guo, R. Y., & Huang, H. J. (2008). A mobile lattice gas model for simulating pedestrian evacuation. Physica A, 387, 580 - 586.

Guo, R.Y., Wong, S.C., Huang, H.J., Zhang, P., & Lam, W. H. (2010). A microscopic pedestrian-simulation model and its application to intersecting flows. *Physica A*, 389, 515 - 526.

Helbing, D., & Molnar, P. (1995). Social force model for pedestrian dynamics. *Physical review E*, 51, 4282 - 4286.

Helbing, D., Farkas, I., & Vicsek, T. (2000). Simulating dynamical features of escape panic. *Nature* 407, 487 - 490.

Helbing, D., Molnar, P., Farkas, I.J., & Bolay, K. (2001). Self-organizing pedestrian movement. *Environment and planning B*, 28, 361 - 384.

Hoogendoorn, S. P., & Daamen, W. (2006). Microscopic parameter identification of pedestrian models and implications for pedestrian flow modeling. *Transportation Research Record: Journal of the Transportation Research Board*, 1982, 57 - 64.

Ko, M., Kim, T., & Sohn, K. (2013). Calibrating a social-force-based pedestrian walking model based on maximum likelihood estimation. *Transportation*, 40, 91 - 107.

Okazaki, S. (1979). A study of pedestrian movement in architectural space, Part I: pedestrian movement by the application of magnetic models. *Trans. A.I.J.*, 283, 111 - 119.

Robin, T., Antonini, G., Bierlaire, M., & Cruz, J. (2009). Specification, estimation, and validation of a pedestrian walking behavior model. *Transportation Research Part B*, 43, 36 - 56.

Seyfried, A., Steffen, B., & Lippert, T. (2006). Basics of modelling the pedestrian flow. *Physica A*, 368, 232 - 238.

Suzuki, K., & Nakamura, H. (2006). TrafficAnalyzer-the integrated video image processing system for traffic flow analysis, *In: Proceedings of the 13th World Congress on Intelligent Transportation Systems*, London, England.

Zhang, X., Chen, P., Nakamura, H., & Asano, M., 2013. Modeling pedestrian walking speed at signalized crosswalks considering crosswalk length and signal timing. *In: Proceeding of the 10th International Conference of the Eastern Asia for Transportation Studies (EASTS)*, Taipei.